

Reverse osmosis of ammonium and sodium salt solutions and its model description

Stanisław Koter^{a,*}, Veronica Ionela Foamete^b, Mirela Alina Constantin^c, Izabela Koter^a

^aFaculty of Chemistry, Nicolaus Copernicus University, 7 Gagarin St., 87-100 Toruń, Poland, email: skoter@umk.pl (S. Koter)

^bApa Nova Bucharest, Intrarea Crinului 7, Rosu village, Chiajna, Ilfov County, Romania

^cNational Research and Development Institute for Industrial Ecology ECOIND, 71-73 Drumul Podu Dambovitei, 060652, Bucharest, Romania

Received 31 March 2018; Accepted 12 June 2018

ABSTRACT

The tested models of membrane transport were based on the steric, dielectric (Born and image force effects), and Donnan exclusions. Generally, the models with the concentration-dependent electrolyte permeability described the retention data satisfactorily, irrespectively of the origin of that dependence (dielectric or Donnan effect). Regarding the steric-dielectric exclusion, the same goodness of fit was obtained for many pairs of pore radius and dielectric constant. However, it was not possible to explain the differences in the electrolyte permeabilities, because of the inconsistency of the dielectric constant of a pore solution and/or an effective membrane thickness. Much too high values of that thickness obtained for the pure Donnan exclusion indicated that this type of exclusion was of marginal importance.

Keywords: Reverse osmosis; Ammonium salts; Dielectric exclusion; Nernst–Planck equation

1. Introduction

Reverse osmosis (RO) and nanofiltration are important membrane techniques used in many fields (chemical, food, pharmaceutical, and paper industries) [1]. The treated solutions are mainly aqueous electrolytes or neutral species, but they can also be organic [2]. To optimize the process, an efficient model should be developed. Such a model should cover three issues: a membrane transport, mass transfer in a membrane module, and a process scale-up [3]. Being aware of a variety of treated wastewaters, industrial effluents and groundwaters, an appropriate description of membrane transport, which is confirmed by the abundant literature on that subject, seems to be the most challenging.

The membrane transport in NF processes can be modeled using the linear transport equations of nonequilibrium thermodynamics [4,5], frictional model of transport [6], extended Nernst–Planck (ENPE) [7–11], and Maxwell–Stefan

equations [3,12]. Various approaches to the partition of electrolytes between a membrane and an external solution are applied – Donnan exclusion [6,7,10,13,14], steric exclusion [8,10,13,14], dielectric exclusion, which comprises of the Born solvation energy difference [9,13,14] and the image force contribution [5,13–17]). In the pore model, the radial distribution of ions inside the pore is sometimes considered [5,8], however, the quantities (concentration, velocity, and electric potential) averaged over a pore cross-section are mostly used. More detailed comments to these approaches can be found in Refs. [16,17]. The hindrance factors for diffusion and for convection, being a function of the ionic to pore radius ratio, are also commonly used.

Reviewing the results of model verifications, for each model one can find experimental examples, where it works or fails. For example, the Donnan Pore Model (DPM) model (DPM = ENPE + Donnan exclusion + hindrance factors depending on the pore radius, r_p) turned out to be satisfactory in fitting the data concerning the filtration of NaCl, Na₂SO₄

* Corresponding author.

and their mixture through various NF membranes covering the range from ultrafiltration to RO, as reported by Bowen and Mukhtar [18]. Two fitted parameters of that model were r_p and charge density. The DSPM model (Donnan Steric Pore Model) was tested by Bowen et al. [8,9] – for monovalent salts (LiCl, NaCl, and KCl) it yielded good results, but it was invalid for a divalent cation salt (MgCl_2). Similarly, Vezzani and Bandini [16,19] found that DSPM was applicable for monovalent cation salts, however, in the case of divalent cations (CaCl_2 , MgCl_2 , and MgSO_4) it failed. The incorporation of the dielectric exclusion resulting from the image force effect (DSPM-DEi, dielectric constant of pore solution, ϵ_p , was the same as that of the external one) substantially improved the fit of these salts, however, still it was far from ideality. In the case of NaCl- Na_2SO_4 mixture [16], the differences between DSPM and DSPM-DEi were practically insignificant. Regarding the Donnan exclusion, Vezzani and Bandini [19] assumed that the membrane was highly charged and the counter-ion concentration could be approximated by that of fixed charges. However, the obtained expression for the fixed charge concentration (Tab. 2 in Ref. [19]) denied it. The DSPM-DEB model (with Born effect, no image force contribution) was examined in Refs. [9,20,21]. Hagemeyer and Gimbel [20] assuming that ϵ_p was concentration dependent, obtained a relatively good fit of single salts (NaCl, Na_2SO_4 , and CaCl_2) and a poorer fit for their mixtures, for example, the negative rejection of Na^+ in the case of NaCl/ CaCl_2 filtration could not be predicted. Bowen and Welfoot [9] (here ϵ_p depended on r_p) found that the standard error of the estimated rejection coefficient of the DSPM-DEB fit for NaCl was 3–10 times worse than that of DSPM (Tab. 3 in Ref. [9]), whereas for MgCl_2 it was better, however not for the lowest feed concentration (ca. 1 mM, Tab. 4 in Ref. [9]). One could also notice that DSPM-DEB yielded much smaller concentration of fixed charges comparing with DSPM indicating a significant DE contribution to the electrolyte exclusion. The DSPM-DEB model, as described in Ref. [9], was tested by Santafé-Moros et al. [21] for the salt mixtures – they obtained a good fit for the mixture $\text{NO}_3^-/\text{SO}_4^{2-}/\text{Na}^+$, but unsatisfactory for $\text{NO}_3^-/\text{Cl}^-/\text{Na}^+$. Escoda et al. [22] successfully applied DSPM-DEB for the filtration of mono- and divalent cations mixture (NaCl- CaCl_2) of various salts ratios. The DSPM-DE model with both effects of dielectric exclusion (Born, image force contributions) was tested by Szymczyk et al. [13,17]. In Ref. [13], a good fit of single salts KCl and MgCl_2 was reported. Regarding salts with divalent cations ($\text{Pb}(\text{NO}_3)_2$ and $\text{Co}(\text{NO}_3)_2$) [17], the authors found that the experimental rejection was well described using either the Born dielectric effect or the image forces contribution. Surprisingly, using both types of dielectric exclusion the data fit was unsatisfactory. To eliminate the fixed charges contribution and to discuss the dielectric effects only, Oatley et al. [23–25] performed the filtration experiments at the isoelectric point of membranes determined from the zeta potential. The results were not unequivocal – in Refs. [23,24] they confirmed the validity of the Born approach, whereas in Ref. [25] they suggested that image force effect could provide a better description.

Thus, the conclusions about the validity of the models, including the type of dielectric exclusion, are not so obvious. Moreover, in the papers dealing with the image force contribution, the conventional form of ENPE is used for description

of transport inside the membrane pores. However, as this contribution depends on concentration, the driving force in the ENPE should include this dependence (details will be provided further), which may change fitting results. Operating on hypothetical (virtual) external solutions instead of pore solutions, this problem disappears. As the image dielectric exclusion depends strongly on cavity geometry [15], another question is which shape of membrane pore should be chosen. In literature, a complex irregular pore geometry is approximated by two ideal cases – cylindrical pores [13,14] and slit-shaped ones [13,16,17,19]. It seems that cylindrical geometry would be more realistic than the slit, however, regarding the pore entrance it is not necessary true [25]. Moreover, it should be stressed that according to Yaroshchuk [15,26], the derived formulas for the image dielectric exclusion are based on simplifying assumptions and should be treated with care.

In this paper, we apply the transport models with and without dielectric exclusion for the description of the filtration data obtained for the monovalent cation salts and a commercial RO membrane. The chosen electrolytes are NH_4Cl , NH_4NO_3 , $(\text{NH}_4)_2\text{SO}_4$, NaCl, NaNO_3 , and Na_2SO_4 . The reason for the choice of nitrogenous compounds is that, for example, nitrates are dangerous for humans or aquatic animals and their content in wastewater, groundwater, drinking water should be reduced [10,21,27,28]; ammonium nitrate and sulfate are fertilizers, which can be recovered from wastewater using membrane filtration [29–31], etc. Among many possible transport models, we selected two models of an uncharged membrane and one of a charged membrane. The first one is the Spiegler–Kedem–Katchalsky (SKK) model based on the nonequilibrium thermodynamics with constant parameters (denoted as the SKK model); here the electrolyte permeabilities is analyzed in terms of the steric and Bohr dielectric exclusion mechanisms. Additionally, it is tested with the electrolyte partition coefficient expressed by Freundlich or Langmuir isotherms (cSKK model). The second model is based on the electrolyte partition depending on the steric, Born, and image force effects (SPM-DE model). In the third one, the electrolyte partition is given by the Donnan effect (DPM model). The main goal is to verify whether a consistent description of all six electrolytes can be obtained. For the electrolyte permeabilities, a common parameter is the membrane geometric parameter defined as the ratio of the pore length to the surface porosity. A special attention is given to the thickness of the polarization layer – three methods of its determination are compared (model fitting, volume flux, and mass transfer correlation).

2. Experimental

The filtration was performed using the dead-end SEPA ST cell (Osmonics). The experimental setup is shown in Fig. 1. The filtration cell was not thermostated, the temperature was measured with an electronic thermometer. The magnetic stirrer was Barnstead/Thermolyne Cimarec®.

A membrane sample was cut from the RO membrane module AG-90 produced by GE Water & Process Technologies; it is denoted here as GE-H. Before measurements, the membrane sample was conditioned by filtering distilled water under the pressure 30 bar for at least 1 h until a constant water flow was obtained. The active membrane

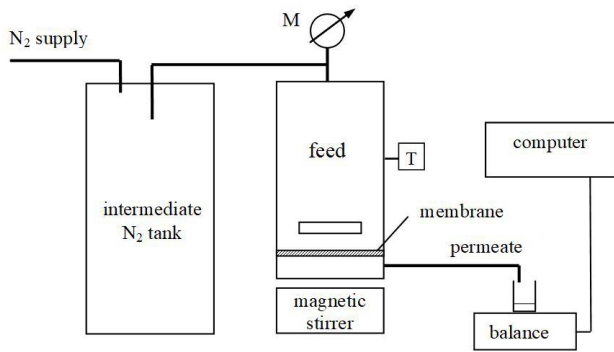


Fig. 1. Experimental setup, *M* – electronic manometer and *T* – thermometer.

area was 12 cm², the initial feed volume was 0.3 L. Each time, before electrolyte filtration, the distilled water was filtered. The time of electrolyte filtration runs and the number of gathered permeate samples are listed in Table 1. The concentration of permeate was determined conductometrically using calibration curves. The observed retention coefficient, $R_{\text{obs},i}$ was calculated from the formula (1):

$$R_{\text{obs},i} = 1 - \frac{c_{p,i}}{\hat{c}_{f,i}} \quad (1)$$

Table 1

Parameters of performed experiments; $c_{f,0}$, $c_{f,\text{end}}$ – initial and final concentration of feed, respectively, Δp – applied pressure, $\Delta T = (T_{\text{max}} - T_{\text{min}})$ – maximal change of temperature observed during the experiment

Electrolyte	Run no.	Symbol of run	Run time (h)	No. of permeate samples	$c_{f,0}$ (M)	$c_{f,\text{end}}$ (M)	Δp (bar)	T_{min} (°C)	ΔT (°C)
NH ₄ NO ₃	1	0.05–15	10	7	0.05	0.18	15	24.2	3.9
	2	0.05–20	6.5	7	0.05	0.14	20	21.6	5.5
	3	0.1–30	3	8	0.1	0.2	30	25.6	2.1
	4	0.2–30	4	7	0.2	0.39	30	26.3	0.5
NH ₄ Cl	5	0.05–15	10	7	0.05	0.16	15	22.8	1.5
	6	0.05–20	7.5	7	0.05	0.18	20	19.8	6.3
	7	0.1–30	4	8	0.1	0.24	30	24.8	0.7
	8	0.2–30	5	8	0.2	0.44	30	23.2	2.6
(NH ₄) ₂ SO ₄	9	0.1–15	17	7	0.1	0.22	15	22.4	3.5
	10	0.1–20	12	7	0.1	0.27	20	22.9	1.2
NaNO ₃	11	0.1–15	10.5	6	0.1	0.19	15	22.4	1.8
	12	0.1–20	9.5	7	0.1	0.28	20	23.2	1.8
	13	0.1–30	3.5	8	0.1	0.21	30	25.8	1.3
	14	0.2–30	6	10	0.2	0.55	30	26.2	0.8
NaCl	15	0.1–15	11	5	0.1	0.19	15	21.8	1.9
	16	0.1–20	15	7	0.13	0.33	20	21.9	3.1
	17	0.1–30	4	8	0.1	0.22	30	24.8	1.0
	18	0.2–30	5.5	8	0.2	0.4	30	24.4	1.6
Na ₂ SO ₄	19	0.1–15	13	9	0.1	0.16	15	22.4	2.3
	20	0.1–20	11.5	12	0.1	0.22	20	25.1	2.9
	21	0.1–30	8.5	12	0.1	0.28	30	27.1	2.5

where $c_{p,i}$ is concentration of *i*th permeate sample, $\hat{c}_{f,i}$ – mean concentration of feed during gathering that sample; it was calculated as an arithmetic mean of the feed concentrations at the beginning, $c_{f,i-1}$ and at the end, $c_{f,i}$ of gathering the *i*th sample: $\hat{c}_{f,i} = (c_{f,i-1} + c_{f,i}) / 2$, $c_{f,i}$ was calculated from Eq. (2) resulting from the mass balance considerations:

$$c_{f,i} = \frac{1}{m_{f,0} - \sum_{j=1}^i m_{p,j}} \left(m_{f,0} c_{f,0} - \sum_{j=1}^i m_{p,j} c_{p,j} \right), \quad i = 1 \dots n \quad (2)$$

where $m_{f,0}$ is the feed mass at the beginning of filtration, $m_{p,j}$ is the mass of *j*th permeate sample. The conditions of performed filtration experiments are listed in Table 1.

In order to verify whether the membrane surface was charged and, consequently, whether the application of the fixed charge model is justified, the streaming potential was measured using a setup consisting of the measurement cell with an electrolyte solution flowing along the membrane surface (see, e.g., Fig. 4b in Ref. [32]), the multimeter Keithley 2700 with the differential multiplexer 7710, the pressure transducer Validyne, and the Gilson peristaltic pump.

3. Theory

For the quantitative description of experimental results, two transport equations are used. The first one is the

Kedem–Katchalsky–Spiegler equation derived from the linear transport equations of nonequilibrium thermodynamics. It describes the flux of a species (uncharged solute or electrolyte consisting of one kind of anion and cation), J_s [4]:

$$J_s = -P_s \frac{dc}{dx} + S_v c J_v \quad (3)$$

where c is concentration of hypothetical solution at equilibrium with the membrane at the point x , J_v – volume flux, and P_s – solute permeability. The parameter S_v is defined as $S_v \equiv 1 - \sigma$, where σ is reflection coefficient. In this work, the coordinate x is dimensionless, scaled with respect to the pore length l_p ; it means that P_s includes l_p .

The second transport equation, which describes the movement of ions, is the ENPE Eq. (4) frequently used in the modeling of electrolyte filtration (e.g., Refs. [7–10]):

$$J_i = -\frac{\bar{D}_i}{\delta} \left(\frac{d\bar{c}_i}{dx} + z_i \bar{c}_i \frac{F}{RT} \frac{d\bar{\varphi}}{dx} \right) + K_{c,i} \bar{c}_i J_v, \quad i = 1, 2 \quad (4)$$

In Eq. (4), J_i is the flux of ion i per unit membrane area, \bar{c}_i , \bar{D}_i , z_i , and $\bar{\varphi}$ denote concentration, diffusion coefficient, charge number of ion i , and electric potential in the membrane pore solution, respectively, $K_{c,i}$ is hindrance convection coefficient of ion i [7] (convection factor in Ref. [33]), δ is the effective membrane thickness [16,19] defined as $\delta \equiv l_p / X_p$, where X_p is the surface fraction of pores. In a more general form Eq. (4) can be written as:

$$J_i = -\frac{\bar{D}_i \bar{c}_i}{\delta RT} \frac{d\bar{\mu}_i}{dx} + K_{c,i} \bar{c}_i J_v = -\frac{\bar{D}_i \bar{c}_i}{\delta RT} \frac{d\bar{\mu}_i}{dx} + K_{c,i} \bar{c}_i J_v \quad (5a,b)$$

where $\bar{\mu}_i$ in Eq. (5a) is the electrochemical potential of ion i inside the membrane, $\bar{\mu}_i$ in Eq. (5b) refers to an external hypothetical solution (also called a virtual one [37]) defined by the equality $\bar{\mu}_i = \bar{\mu}_i^*$. Then Eq. (5b) can be transformed into (3), where P_s and S_v are given by:

$$P_s = P_{s,u} A \quad (6a)$$

$$S_v = S_{v,u} A \quad (6b)$$

A , $P_{s,u}$, and $S_{v,u}$ are defined as:

$$A = \frac{z_1 - z_2 k_D}{z_1 / K_{p,2} - z_2 k_D / K_{p,1}} \quad (7)$$

$$P_{s,u} = \frac{(z_1 - z_2) \bar{D}_2}{(z_1 - z_2 k_D) \delta} \left(1 + \frac{d \ln \gamma_{\pm}}{d \ln c} \right) \quad (8a)$$

$$S_{v,u} = \frac{z_1 K_{c,2} - z_2 K_{c,1} k_D}{z_1 - z_2 k_D} \quad (8b)$$

where k_D is the diffusivity ratio, $k_D \equiv \bar{D}_2 / \bar{D}_1$. The hindered by the presence of pore walls diffusion coefficient of ion i in the pore solution, \bar{D}_i , is related to that in a free solution, D_i , by $\bar{D}_i = K_{d,i} D_i$ [7], where $K_{d,i}$ is hindrance diffusion coefficient. Both $K_{d,i}$ and $K_{c,i}$ depend on the ratio of solute to pore radius (Refs. [7,13,34]). The partition coefficient of ion i , $K_{p,i}$,

results from the equality of its electrochemical potentials at the membrane/solution boundary, $\bar{\mu}_i = \tilde{\mu}_i$. It depends on many factors, which are summarized in Eq. (9) [13]:

$$K_{p,i} \equiv \frac{\bar{c}_i}{c_i} = \frac{\gamma_i}{\tilde{\gamma}_i} \Phi_i \exp(-z_i F \Delta \varphi / RT - \Delta W_{B,i} - W_{im,i}) \quad (9)$$

where γ_i and $\tilde{\gamma}_i$ are ion activity coefficients outside and inside the membrane, respectively, $\Delta \varphi$ is a difference in electric potential inside and outside the membrane (it includes the Donnan potential if the fixed charges are present), $\Delta W_{B,i}$ is a change in solvation energy (divided by RT) resulting from the transfer of ion i from the external solution of dielectric constant ϵ to the membrane pore solution of dielectric constant ϵ_p , $W_{im,i}$ is a contribution of dielectric exclusion resulting from the image forces [15], Φ_i is a steric exclusion term. For NF membranes, it is usually described by the expression for cylindrical pores derived on the base of geometric arguments [35]: $\Phi_i = (1 - r_{s,i} / r_p)^2$, where $r_{s,i}$ is the Stokes radius of ion i , r_p – pore radius. The ion partition coefficients, $K_{p,1}$ and $K_{p,2}$, are not independent quantities – they are connected with each other by the electroneutrality condition inside the membrane:

$$z_1 \bar{c}_1 + z_2 \bar{c}_2 + X_m = 0 \quad (10)$$

where $X_m \equiv z_m \bar{c}_m$, \bar{c}_m is concentration of fixed charges, z_m – their charge number.

A relation between J_v and the concentration of the feed at the membrane surface, c_m , and of permeate, c_p , results from the equality $J_s = c_p J_v$ ($J_s = \text{constant}$), which when combined with Eq. (3) gives the basic Eq. (11) for the discussed models:

$$J_v = - \int_{c_m}^{c_p} \frac{P_s}{c_p - S_v c} dc \quad (11)$$

where c_m is not known from the direct measurements; it can be determined in different ways basing on the equation resulting from the stagnant film model of concentration polarization [36]:

$$c_m = c_p + (c_f - c_p) \exp(J_v / k_c) \quad (12)$$

where c_f is the bulk feed concentration, k_c is the mass transfer coefficient defined as the ratio of the salt diffusivity, D_s , to the thickness of concentration polarization layer, l_{pol} ($k_c = D_s / l_{pol}$). In the utmost situation, one can neglect the polarization effect, as it was done by Hagemeyer and Gimbel [20]. Other authors (e.g., Refs. [8,23]) prefer a rather laborious method of determining the real rejection coefficient, R , directly related to c_m (Eq. (14)); the method is based on the assumption that R does not depend on the stirrer speed (dead-end mode) or cross-flow velocity of feed (cross-flow mode). It is not so obvious because R is a function of concentration at the membrane surface, which depends on the hydrodynamic conditions. Some other authors use the correlation equations for k_c [10]. In this work, k_c and, consequently, l_{pol} were determined from the model fitting. A comparison with k_c obtained from the correlation for a stirred cell and from the expression for volume flux (Eq. (26)) is given in the Supplementary information.

Regarding the integral (Eq. (11)) relating J_v with the membrane parameters, P_s and S_v , four cases were considered, denoted as the SKK, cSKK, SPM-DE, and DPM models.

3.1. The SKK model

The simplest case (SKK model) is based on the assumption $P_s, S_v = \text{constant}$, which applied to Eq. (11) yields:

$$J_v = \frac{P_s}{S_v} \ln \left(\frac{(1-R)(1-S_v)}{1-R-S_v} \right) \quad (13a)$$

$$(J_v)_{S_v=0} = \frac{P_s R}{1-R} \quad (13b)$$

where R is the real retention coefficient:

$$R \equiv 1 - \frac{c_p}{c_m} \quad (14)$$

Because for the investigated membrane, a convective term in the solute flux turned out to be of minor importance, the formula for $S_v = 0$ is also shown. In this model, P_s can be further interpreted in terms of Eqs. (6a)–(9) under the assumption that $K_{p,i}$ does not depend on concentration. It means that here only the steric and Born exclusion can be taken into account.

3.2. The cSKK model

In accordance with the definitions of $A, P_{s,u}$ and $S_{v,u}$ (Eqs. (7) and (8a,b)), one can expect that $P_{s,u}$ (neglecting the term with γ_{\pm}) and $S_{v,u}$ should be more or less constant, whereas A for uncharged membrane is just the electrolyte partition coefficient, K_p , and should be concentration dependent. Analyzing this term in view of the Donnan equation (23), one can find that the simplest function describing concentration dependence of A ($=K_p$) would be just the same expression as Freundlich or Langmuir isotherms: $A \propto c^n$, $A \propto c/(a+c)$, where n and a are fitting parameters. The first dependence $A(c)$ corresponds to that resulting from the ideal Donnan equation (23) for the condition $c \ll \bar{c}_m$, where \bar{c}_m is the concentration of fixed charges. For that case $n = -z_{\text{cation}}/z_{\text{counterion}}$ [37]. The dependence $A \propto c/(a+c)$ sets the limit of A for $c \rightarrow \infty$, similarly as Eq. (23). Substituting $A \propto c^n$ into Eq. (6) we get:

$$P_s = P_{s,0} \left(\frac{c}{c^*} \right)^n \quad (15a)$$

$$S_v = S_{v,0} \left(\frac{c}{c^*} \right)^n \quad (15b)$$

where c^* (≈ 1 M) has been introduced to ensure the same unit of P_s and $P_{s,0}$ (similarly for S_v). $P_{s,0}$ and $S_{v,0}$ are not the same as $P_{s,u}$ and $S_{v,u}$; they contain proportionality factor between A and $(c/c^*)^n$. Eqs. (15a,b) substituted into Eq. (11) lead to [38]:

$$J_v = \frac{P_{s,0}}{(1+n)S_{v,0}} \ln \left(\frac{(1-R)(1-(1-R)S_{v,0}(c_m/c^*)^n)}{1-R-S_{v,0}(c_m/c^*)^n} \right) \quad (16a)$$

$$(J_v)_{S_v=0} = \frac{P_{s,0}(1-(1-R)^{1+n})}{(1+n)(1-R)} \left(\frac{c_m}{c^*} \right)^n \quad (16b)$$

Analogous expression for J_v can be derived for $A \propto c/(a+c)$; for $S_v = 0$ it takes a simple form:

$$(J_v)_{S_v=0} = P_{s,0} \left(\frac{R}{a(1-R)} - \frac{1}{c_p} \ln \left(\frac{1+ac^*/c_m}{1+ac^*/c_m-R} \right) \right) \quad (17)$$

3.3. The SPM-DE model

The SPM-DE model is based on the assumption that the concentration of solute inside the membrane is governed by Eq. (9). In that case, the electrochemical potential of an ion in the membrane pore solution, $\bar{\mu}_v$, includes the image force term, $W_{\text{im},v}$ which is concentration dependent [13]. Thus, in Eq. (5a) the driving force is:

$$\frac{d\bar{\mu}_i}{dx} = RT \frac{d \ln \bar{a}_i}{dx} + z_i F \frac{d\bar{\phi}}{dx} + \frac{dW_{\text{im},i}}{dx} \quad (18)$$

and, consequently, in Eq. (4) the driving force should include the term $\bar{c}_i dW_{\text{im},i} / dx$, which makes the use of Eqs. (4) and (5a) less comfortable. Using the external hypothetical solution approach (Eqs. (5b) or (3) with P_s and S_v given by Eqs. (6a,b)) this term disappears. To avoid the excessive model parametrization, it is further assumed that the membrane is uncharged ($X_m = 0$ in Eq. (10)) and, consequently, $K_{p,1} = K_{p,2}$. In that case P_s and S_v become:

$$P_s = P_{s,u} K_p \quad (19a)$$

$$S_v = S_{v,u} K_p \quad (19b)$$

where K_p can be expressed as:

$$K_p = K_{p,1}^{z_1 - z_2} K_{p,2}^{z_1 - z_2} = \frac{\gamma_{\pm}}{\bar{\gamma}_{\pm}} \Phi_1^{z_1 - z_2} \Phi_2^{z_1 - z_2} \exp \left(- \frac{z_1 - z_2 r_{\text{cav},1} / r_{\text{cav},2} \Delta W_{B,1}}{(z_1 - z_2) z_1 / z_2} \right) \exp \left(\frac{z_2}{z_1} W_{\text{im},1} \right) \quad (20)$$

Eq. (20) was derived from Eq. (9) by eliminating $\Delta\phi$ using the electroneutrality condition (10) and applying the relations:

$$\frac{\Delta W_{B,2}}{\Delta W_{B,1}} = \frac{r_{\text{cav},1} z_2^2}{r_{\text{cav},2} z_1^2} \quad (21a)$$

$$\frac{W_{\text{im},2}}{W_{\text{im},1}} = \left(\frac{z_2}{z_1} \right)^2 \quad (21b)$$

resulting from the definitions of $\Delta W_{B,i}$ and $W_{\text{im},i}$ (Eqs. (9) and (10) in Ref. [13]). The activity coefficient ratio, $\gamma_{\pm} / \bar{\gamma}_{\pm}$ can be treated in various ways – in Ref. [15] it was expressed as the limiting Debye–Hückel law, in Refs. [13,39] the extended Debye–Hückel equation was used, in Ref. [14] it was neglected. It should be noted that the dependence of K_p on the dielectric constant of pore solution, ϵ_p is not so obvious, because the Born contribution ($\Delta W_B \propto 1/\epsilon_p - 1/\epsilon_B$) increases when ϵ_p decreases, whereas in the case of image forces the situation is opposite – the higher ϵ_p comparing with ϵ_m the higher exclusion. Because of complicated dependence of

$W_{im,1}$ and, consequently, K_p on c , it is not possible to obtain an analytical solution of Eq. (11). The procedure applied here was as follows – at first for given values of pore radius, r_p , and dielectric constant of pore solution, ϵ_p , the dependence of K_p on c was determined and interpolated by a cubic spline, then it was used in Eq. (11) to calculate J_v . It can be noticed that for $K_p = \text{constant}$ (only steric and Born effects are in Eq. (9)) the model simplifies to SKK. It should be also noticed that as $W_{im,i}$ depends on the concentration of pore solution, it depends also on other factors affecting the partition coefficient, here Φ_i and $\Delta W_{B,i}$. $r_{cav,i}$ needed for the evaluation of $\Delta W_{B,i}$ is the radius of cavity, which ion i forms in a solvent; a precise definition can be found in Refs. [40,41]. In our calculations, the values of $r_{S,i}$ (0.184, 0.125, 0.121, 0.129, and 0.23 nm for Na^+ , NH_4^+ , Cl^- , NO_3^- , and SO_4^{2-} , respectively) were taken from Ref. [42], r_{cav} of Na^+ (0.168 nm), NH_4^+ (0.213 nm), and Cl^- (0.1937 nm) – from Ref. [40], r_{cav} of SO_4^{2-} (0.254 nm) – from Ref. [41]. r_{cav} of NO_3^- (0.2155 nm) were calculated as the sum of covalent radius (0.264–0.14 = 0.124 nm [42]) and the half distance between nitrate oxygen atom and hydrogen atom of water surrounding nitrate (0.183/2 = 0.0915 nm [43]). Other model parameters – the dielectric constant of solutions bathing the membrane, ϵ_p , and of the membrane pore walls, ϵ_m , needed to calculate W_{im} – were assumed to be: $\epsilon_b = 78$, $\epsilon_m = 6$. The last value is higher than ϵ of the membrane forming polymers (ca. 3 [44]); it is equal to ϵ of the oriented water molecules at the pore walls [9]. Even higher value of ϵ_m (7–10) was obtained by Bouranene et al. [17] for a NF polyamide membrane.

3.4. The DPM model

In the DPM model, it is assumed that the membrane is charged, the electrolyte sorption is described by the ideal Donnan equation (23) and the ion transport by the extended Nernst–Planck equation (4). Neglecting the convective term ($K_{ci} = 0$) in that equation, its integration over the concentration inside the membrane leads to:

$$(J_v)_{K_{ci}=0} = \frac{P_{s,u}}{c_p} \left(\bar{c}_{1,m} - \bar{c}_{1,p} + \frac{z_2 X_m (k_D - 1)}{(z_1 - z_2)(z_1 - z_2 k_D)} \ln \left(\frac{z_1 \bar{c}_{1,f} (z_1 - z_2 k_D) - z_2 k_D X_m}{z_1 \bar{c}_{1,p} (z_1 - z_2 k_D) - z_2 k_D X_m} \right) \right) \quad (22)$$

In the derivation of the earlier equation, the electroneutrality condition (10) was applied. A full integrated expression for J_v can be found in Refs. [6,7,45]. $\bar{c}_{1,k}$ is concentration of ion 1 inside the membrane at the boundaries with feed ($k = f$) and permeate ($k = p$). In general, the relation of that concentration with the external concentration on the feed or permeate side is given by Eq. (9) which can also be written as:

$$\bar{c}_1^{-1/z_1} \bar{c}_2^{-1/z_2} = k_{eq} c_1^{1/z_1} c_2^{-1/z_2} \quad (23)$$

where for the pure ideal Donnan sorption $k_{eq} = 1$.

3.5. The model parameters

The fitting model parameters are SKK – l_{pol} , $P_{s,25}$, α_p ; cSKK – l_{pol} , $P_{s,25}$, α_p , n ; SPM-DE – l_{pol} , $P_{s,25}$, α_p , r_p , ϵ_p ;

DPM – l_{pol} , $P_{s,25}$, α_p , X_m . S_v is not included as it was found that for the studied membrane this parameter was negligible. The parameter α_p describes the temperature influence of P_s ($P_{s,0}$ or $P_{s,u}$) expressed by the formula:

$$P_s = P_{s,25} (1 + \alpha_p (T / ^\circ\text{C}) - 25) \quad (24)$$

where $P_{s,25}$ refers to 25°C. Eq. (24) works well in not too large temperature range and there was no need to use the Arrhenius equation here. The diffusion coefficient of electrolytes needed for the estimation of c_m (Eq. (12)) was expressed by the equation analogous to (24) where the temperature coefficient was estimated from the limiting ion conductivities [46]. It should be noted that the membrane cell was not thermostated intentionally because: (1) not always the exact thermostating of membrane module is possible and (2) we wanted to check the importance of temperature coefficient when small temperature changes (below 10°C) during experiments occur.

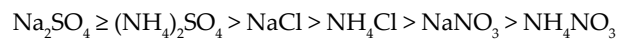
The optimal model parameters were found by minimizing the sum of square errors, SSE:

$$\text{SSE} = \sum_i (J_{v,\text{mod},i} - J_{v,\text{exp},i})^2 \quad (25)$$

In order to avoid meaningless values of S_v and l_{pol} , these quantities were substituted by a sigmoidal function of an auxiliary fitting parameter, which enabled the imposition of a lower and upper limit of S_v (0 and 1) and l_{pol} (10 and 500 μm) (see Supplementary information).

4. Results and discussion

The concentration dependence of the observed retention coefficient, R_{obs} , and of volume flux, J_v , are shown in Figs. 2 and 3, respectively. Generally, R_{obs} and J_v decreased with the feed concentration, however in some cases initially an increase in R_{obs} and J_v was observed (NH_4Cl , Figs. 2 and 3). This effect can be related to the membrane conditioning at the beginning of experiment. For better comparison of electrolyte retentions, the values of R_{obs} for $c_f = 0.1$ M are gathered in Table 2; the ratio of $J_v/\Delta p$ to the water hydrodynamic permeability, $L_{p,w}$, is also shown. The series of R_{obs} was as follows:



Divalent sulfates were rejected to the highest extent and chlorides were rejected better than nitrates. Comparing cations, Na^+ was always better rejected than NH_4^+ . It can be noticed that for ammonium salts the difference in R_{obs} between Cl^- and NO_3^- was substantially higher than that of sodium salts. Sulfate rejection only slightly depended on the kind of the cation. The transmembrane pressure increased the volume flux and, consequently, the retention, as it could be deduced from Eq. (13). The highest increase in $R_{\text{obs}} = f(\Delta p)$ was observed for electrolyte of the lowest retention – NH_4NO_3 .

Regarding $(\text{NH}_4)_2\text{SO}_4$, its retention for the comparable feed concentration range and similar transmembrane pressure was slightly lower than that reported by Carter et al. [31]

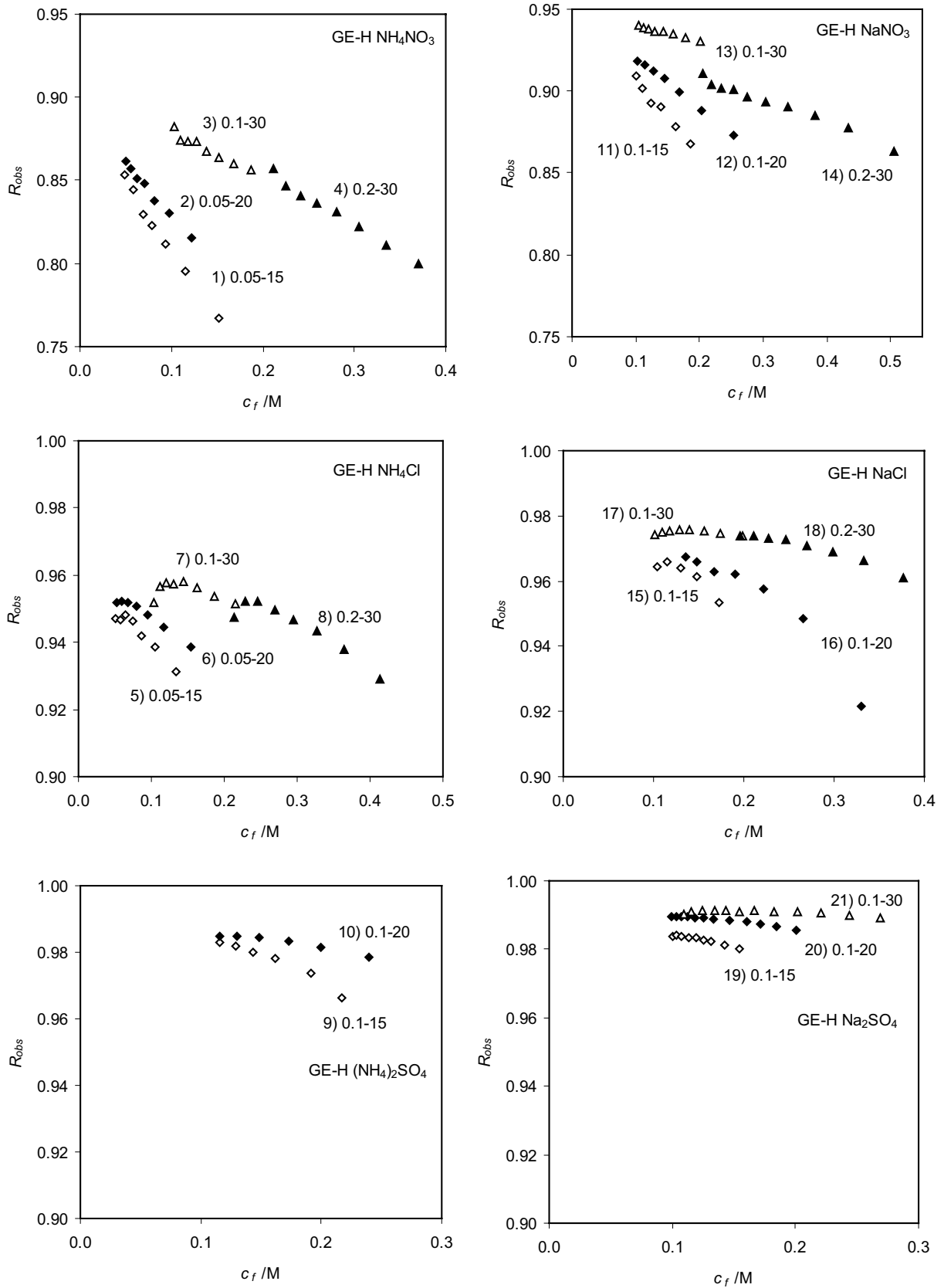


Fig. 2. Observed retention coefficient, R_{obs} , versus concentration of feed, c_f (a mean value while gathering a given sample of permeate), for different initial feed concentrations and pressures (see Table 1).

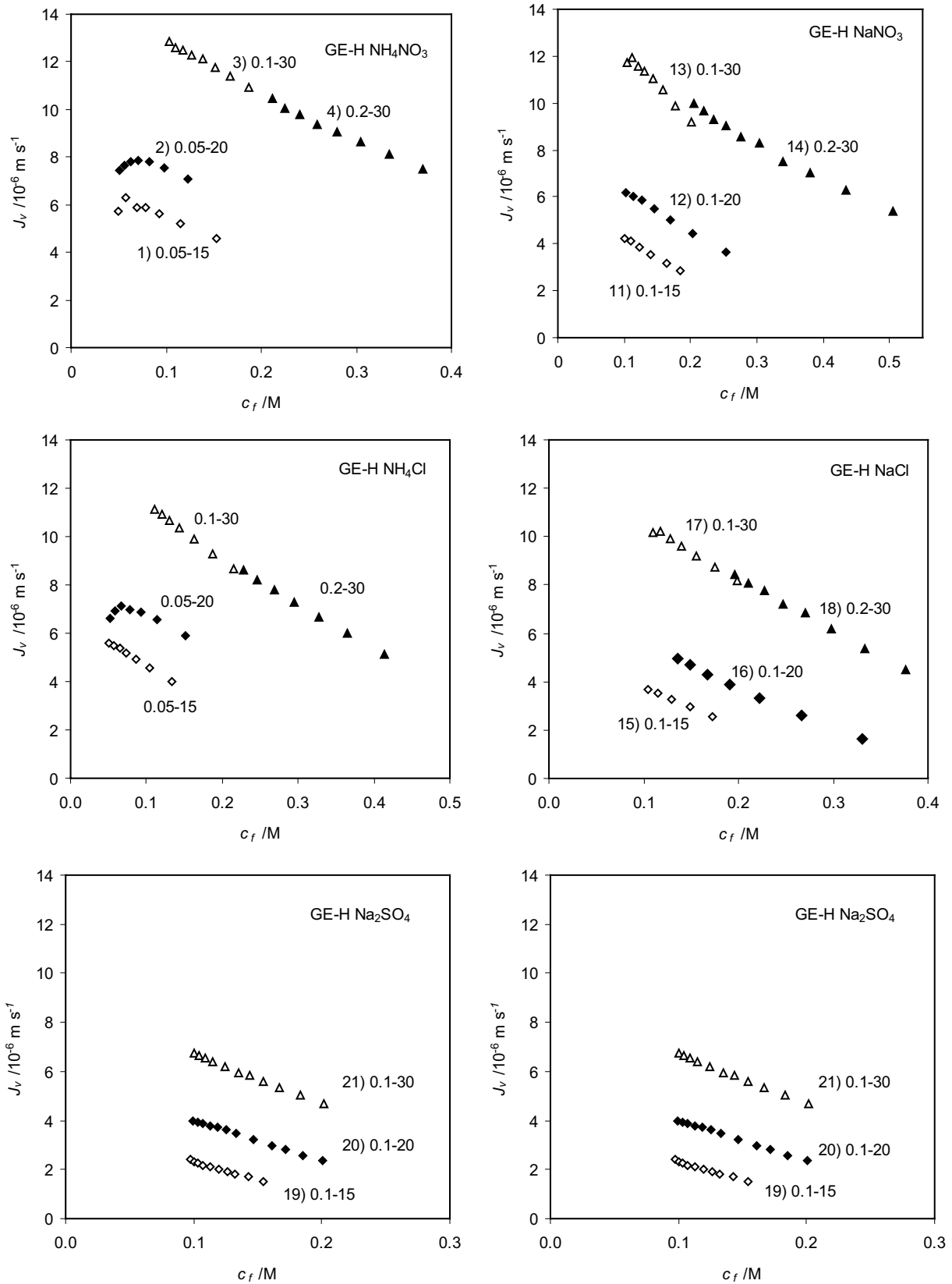


Fig. 3. Volumetric flux, J_v , versus concentration of feed, c_f (a mean value while gathering a given sample of permeate), for different initial feed concentrations and pressures (see Table 1).

Table 2

The observed retention coefficient, R_{obs} , and the volume flux divided by Δp and the water hydrodynamic permeability, $L_{p,w}$, at $c_f = 0.1$ M for different values of transmembrane pressure

Electrolyte	R_{obs}			$J_v/(\Delta p L_{p,w})$		
	15 bar	20 bar	30 bar	15 bar	20 bar	30 bar
NH_4NO_3	0.807	0.830	0.885	0.76	0.78	0.73
NH_4Cl	0.939	0.945	0.952	0.68	0.71	0.78
$(\text{NH}_4)_2\text{SO}_4$	0.983	0.985	–	0.56	0.60	–
NaNO_3	0.909	0.918	0.940	0.63	0.70	0.67
NaCl	0.965	0.967	0.975	0.61	0.67	0.67
Na_2SO_4	0.984	0.990	0.992	0.44	0.56	0.66

for a General Electric polyamide membrane. Contrary to their results, here the retention increased, as expected, with the applied pressure.

In Fig. 2 it can be noticed that for the same $\Delta p = 30$ bar there is a significant discontinuity of the $R_{\text{obs}} = f(c_f)$ curves for NaNO_3 (runs 13 and 14) at the point $c_f \approx 0.2$ M. It is difficult to explain – even a very small leakage through the membrane sealing could cause this effect.

The ratio of $J_v/\Delta p$ to the water hydrodynamic permeability, $L_{p,w}$ (Table 2) is always lower than 1, because of the presence of osmotic pressure difference across the membrane, $\Delta\pi$. This effect is quantitatively described by the equation derived on the basis of linear nonequilibrium thermodynamics [47]:

$$J_v = L_p (\Delta p - \sigma \Delta \pi) \quad (26)$$

Generally, the lower retention, the higher $J_v/(\Delta p L_{p,w})$ because of lower $\Delta\pi$ ($J_v/\Delta p L_{p,w} \approx 1 - \sigma \Delta \pi / \Delta p$). With the increase in pressure, for electrolytes of lower retention (nitrates) $J_v/(\Delta p L_{p,w})$ decreases, because R_{obs} significantly increases with Δp , which means that $\Delta\pi$ should also be substantially increased, thus $\Delta\pi/\Delta p$ is getting higher. For electrolytes of high retention (sulfates), the increase in $\Delta\pi$ is not so high, hence $\Delta\pi/\Delta p$ decreases with Δp which causes the $J_v/(\Delta p L_{p,w})$ gain.

4.1. Model calculations

For the model calculations, the data were “filtered” – the points on the left from the maximum on the $R_{\text{obs}} = f(c_f)$ curve were rejected (e.g., Fig. 2, NH_4Cl , runs 0.1–30 and 0.2–30). The model fitting was performed for single runs and for sets of runs. It was found that the convection part of salt fluxes was negligible in all the models ($S_v \approx 0$). A similar result was observed also for other RO processes, for example, RO of monoborate complexes [48], where the experimentally determined reflection coefficient was higher than 0.999. Thus, as expected, the transport of electrolytes in the investigated membrane has a diffusive character. In single runs the changes in R_{obs} were not so large and all the models fitted the experimental data with a similar accuracy; therefore only the fits of the run sets are further discussed. In that case, the SKK fit was not so satisfactory as that of other models, except for sulfates, in case of which the changes of R_{obs} were very

small (below 0.02). According to the statistic F -test the difference between cSKK and DPM was practically negligible for all electrolytes, the fit of SPM-DE was comparable with those models except nitrates. The temperature coefficient of P_s and α_p was found to be important in the SKK and SPM-DE fits of NH_4NO_3 and NH_4Cl , where the temperature changes were high. The obtained values of α_p from the SPM-DE fit ($\text{NH}_4\text{NO}_3 - 0.031$, $\text{NH}_4\text{Cl} - 0.027$) were slightly higher than those obtained for diffusion coefficients in free aqueous solution (for NH_4NO_3 , NH_4Cl $\alpha_D = 0.023$, 0.024 , respectively, as calculated from the limiting ion conductivities [46]). For other cases α_p was practically negligible.

The experimental R_{obs} values and those resulting from the model fit are compared in Fig. 4 (sets of runs only). The DPM model yielded a similar fit to cSKK and therefore is not shown. For NaNO_3 the run 14 was excluded from the fitting, because of the discontinuity observed in Fig. 2. The model R_{obs} was calculated using the fitted parameters, listed in Table 3, Table S1 (l_{pol}), and the experimental values of J_v/c_f and T . It is seen that for three electrolytes (NH_4NO_3 , NH_4Cl , and NaNO_3) the SKK model ($P_s = \text{constant}$) is worse than the models with P_s dependent on concentration.

It was found that both types of concentration dependence of P_s , $A \propto c^n$ (Eq. (16b)) and $A \propto c/(a+c)$ (Eq. (17)), assumed in the cSKK model, gave similar fit of our experimental data. Therefore, only results for $A \propto c^n$ are shown. The obtained values of the exponent n (Table 3) strongly deviate from $-z_{\text{coion}}/z_{\text{counterion}} = 1$ for 1:1 electrolytes. It means that the condition $c \ll |X_m|$ is not fulfilled – it agrees with small values of X_m obtained from the DPM model. The real rejection coefficient (R , dash symbol in Fig. 4) is substantially higher than R_{obs} and the sequence of electrolytes with respect to R is the same as that for R_{obs} .

Regarding the SPM-DE model, practically the same values of SSE_{min} (Eq. (25)) were obtained for the points (r_p , ε_p) laying on the lines shown in Fig. 5. As it was mentioned above, it is a result of two opposite changes of the electrolyte partition coefficient with ε_p regarding Born and image force effects. The Born exclusion increases, when ε_p decreases, whereas the image exclusion increases with ε_p . Assuming that $\varepsilon_p = \varepsilon_b$ (no Born exclusion), as it was done by Vezzani and Bandini [19], r_p would be between 0.44 nm (NH_4Cl) and 0.50 nm (NaNO_3). These values are ca. 0.2 nm higher than those estimated in Ref. [19] for the nanofiltration N50 membrane (Separex SpA) assuming a slit-like pore geometry and a constant electric potential gradient inside the membrane. Generally, the value of r_p depends on the applied model – in another work with the same membrane Bandini and Vezzani [16] using the Donnan-steric-pore model and different procedures obtained $r_p = 0.4\text{--}0.67$ nm. The assumption – ε_p close to ε_b – could be supported by Escoda et al. [49] who for a polyamide NF membrane, from the membrane potential measurements, obtained $\varepsilon_p = 76$ ($\varepsilon_b = 78.5$, $r_p = 0.93$ nm). However, it is a question whether ε_p so close to ε_b is reliable. Certainly, regarding the radial direction of pore, it is not true. For $r_p \approx 1$ nm and r_{cav} of ions ca. 0.2 nm, only three layers of H_2O between ion and pore wall are possible. The water molecules which are in contact with the pore wall or with an ion are more or less oriented, which results in a low dielectric constant (for completely oriented H_2O molecules $\varepsilon = 6$ [9,50]). Only the intermediate layer of water has higher dielectric constant.

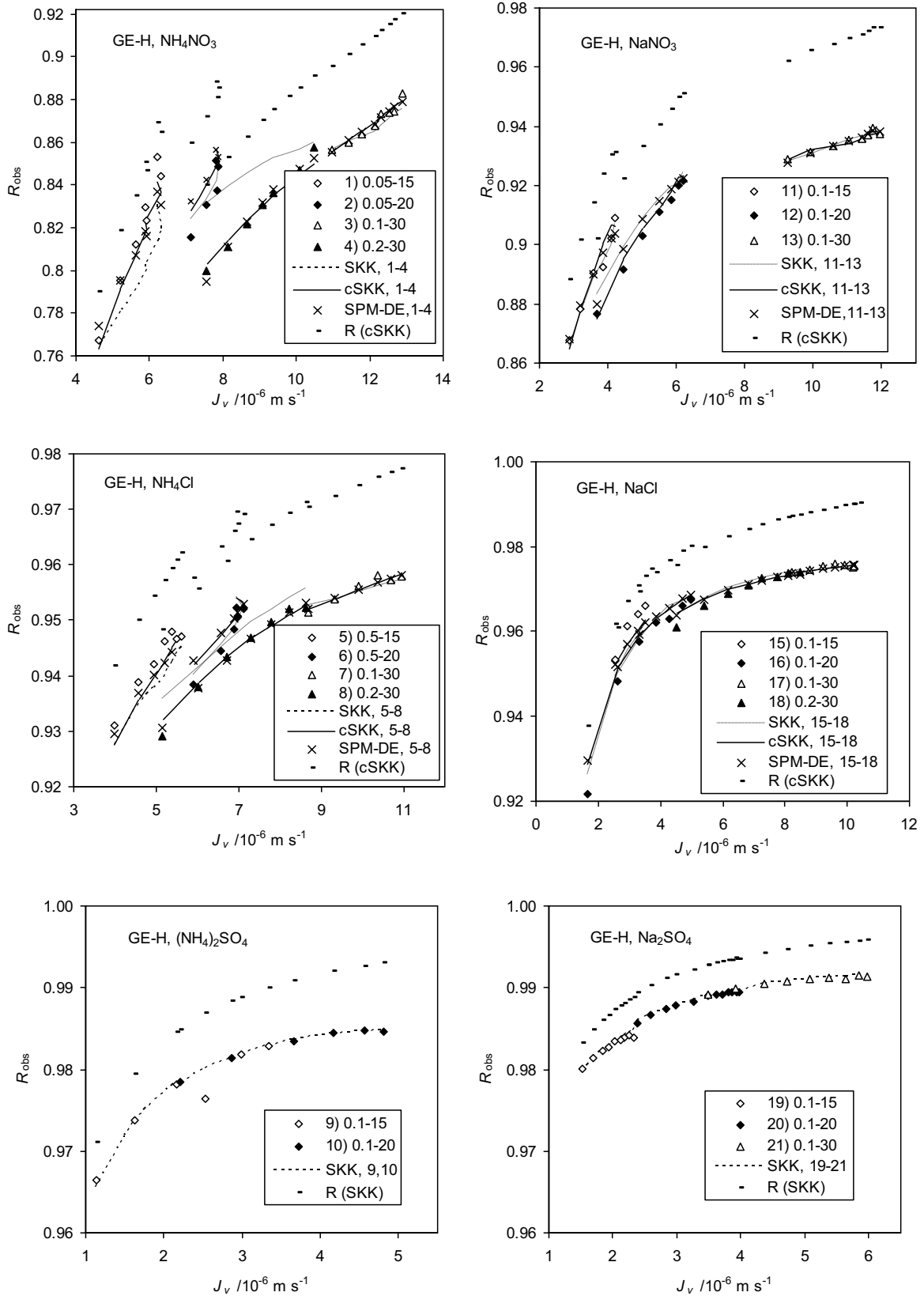


Fig. 4. R_{obs} versus J_v for various feed concentrations and pressures; symbols represent the experimental point, the lines connect the points calculated from the fitted model parameters and the experimental data of J_v , c_p and T , the numbers after the model abbreviation are the run numbers taken for the model fitting; dash symbol – real rejection coefficient.

Table 3

P_s , n , and X_m for the set of runs shown in Fig. 4; “x” means that a model does not yield a statistically better fit than SKK

Electrolyte	P_s ($\mu\text{m/s}$)				n (cSKK)	X_m (DPM) (M)
	SKK (P_s)	cSKK ($P_{s,0}$)	DPM ($P_{s,u}$)	SPM-DE ($\epsilon_p = \epsilon_{p'} P_{s,u}$)		
NH_4NO_3	1.1 ± 0.1	1.9 ± 0.1	1.5 ± 0.1	151	0.19 ± 0.02	-0.076 ± 0.005
NH_4Cl	0.27 ± 0.02	0.32 ± 0.02	0.28 ± 0.01	59	0.09 ± 0.02	-0.036 ± 0.006
$(\text{NH}_4)_2\text{SO}_4$	0.034 ± 0.001	x	x	x	x	x
NaNO_3	0.43 ± 0.02	0.60 ± 0.04	0.43 ± 0.02	35	0.23 ± 0.03	-0.14 ± 0.02
NaCl	0.12 ± 0.01	0.13 ± 0.01	0.12 ± 0.01	26	0.11 ± 0.03	-0.10 ± 0.02
Na_2SO_4	0.026 ± 0.001	x	x	x	x	x

Regarding the axial direction of pore, ions are separated by a large number of H_2O molecules and ϵ should be substantially higher. These considerations are supported by Itoh and Sakuma [51], who determined the dielectric constant of water confined between two graphite slabs using the MD simulations. They found that dielectric constant in the direction perpendicular to the slabs, ϵ_{\perp} , was much lower than that in the parallel direction, ϵ_{\parallel} . For the distance between slabs 1.3 nm they obtained $\epsilon_{\perp} \approx 3.9$ and $\epsilon_{\parallel} \approx 41$. Thus, for the calculation of W_{im} (image force effect) ϵ_p closer to ϵ_{\perp} should be used, whereas in the calculation of ΔW_{B} (Born solvation energy change) some average of ϵ_{\perp} and ϵ_{\parallel} would be more appropriate. It should be noted that from the fitting of the 0.1 M NaCl filtration data ($R = f(J_p)$) Deon et al. [52] obtained $\epsilon_p = 54$ which was lower than that in Ref. [49] ($\epsilon_p = 76$); in both works the same membrane was investigated. In the case of CaCl_2 ϵ_p decreased to 40 because of a stronger electric field of divalent cation Ca^{2+} ordering H_2O molecules to a greater extent.

The observed in Fig. 5 relation ϵ_p (nitrates) $>$ ϵ_p (chlorides) is opposite to that observed for free solutions (sodium salts:

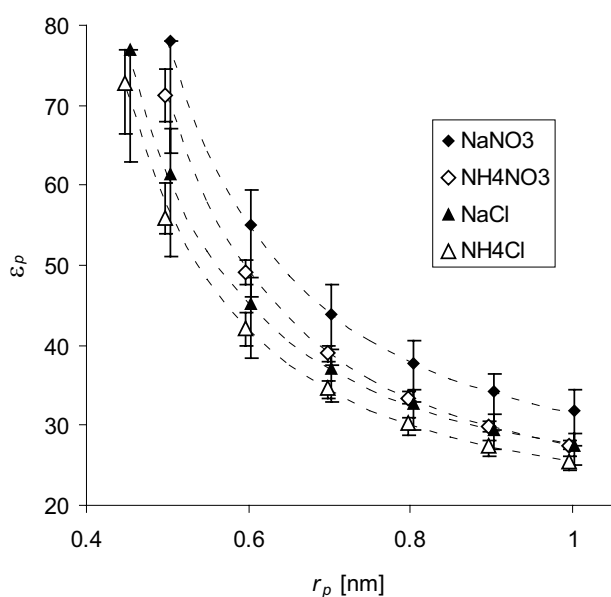


Fig. 5. The SPM-DE model (activity coefficients are omitted): relation between ϵ_p and r_p which gives the same SSE_{min} ; the deviations correspond to the SSE_{min} increased by 10%; and dotted line is for eye guide.

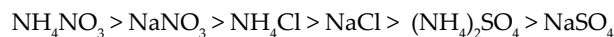
Figs. 9 and 11 in Ref. [53]). With the increase in r_p , the discrepancy between the values of ϵ_p decreases, for example, $r_p = 0.9$ nm $\epsilon_p(\text{NaCl}) \approx \epsilon_p(\text{NH}_4\text{NO}_3) = 30$, $\epsilon_p(\text{NH}_4\text{Cl}) = 27.4$ and $\epsilon_p(\text{NaNO}_3) = 34.2$. Assuming the 10% tolerance of SSE_{min} , the ϵ_p range for NaCl overlaps with that for NaNO_3 , however, this is not so in the case of ammonium salts.

To determine which pair (r_p , ϵ_p) is close to reality, additional experiment is needed. Regarding r_p , a filtration of neutral solute would be helpful [8,19], however, to find a solute of appropriate molecular geometry and properties may not be possible. More information on ϵ_p can bring the electrochemical impedance spectroscopy measurement performed on the isolated active layer [54]. Montavillo et al. [55], for a polyamide NF membrane (Desal HL, Osmonics) in KCl solutions, using the impedance spectroscopy technique, obtained ϵ_p equal ca. 10 for $c \geq 0.001$ M (cylindrical pore). In their calculations, the permittivity of the membrane material was neglected and the mean pore radius was assumed to be 0.48 nm, as determined by Hussain et al. [56] from the filtration of uncharged solutes. In their approach, ϵ_p was directly proportional to r_p^2 ; taking r_p equal to 0.85 nm, ϵ_p would increase to ca. 31 close to our results (Fig. 5).

4.1.1. Electrolyte permeability, P_s , and effective membrane thickness, δ

The optimal values of P_s for the set of runs, seen in Fig. 4, are listed in Table 3 together with the parameters responsible for the concentration dependence of P_s – the exponent n (cSKK) and the fixed charge concentration, X_m (DPM). To be consistent with the preliminary streaming potential measurement results, here the negative values of X_m are given. However, also positive X_m yields a similar model fit. The permeability coefficient of the SPM-DE model, $P_{s,u}$ is shown only for the limiting case $\epsilon_p = \epsilon_b$ (no Born exclusion).

One can notice that the values of solute permeability given by the SKK and DPM models do not differ too much, whereas SPM-DE yields much higher values of P_s because of high electrolyte exclusion predicted by that model. As expected, the sequence of P_s agrees with the reversed sequence observed for R_{obs} (Table 2):



Below, the consistency of P_s and effective membrane thickness for these electrolytes is discussed.

4.1.1.1. The SKK model

The analysis of P_s obtained from the SKK model can be performed assuming that $K_{p,1} = K_{p,2} = \text{constant}$. In that case, only the concentration independent effects (steric and Born, r_p and ϵ_p are constant here) in K_p may be considered. According to Eqs. (8a) and (19a), assuming the same effective membrane thickness, δ , for all electrolytes, the partition coefficient ratio of electrolytes I and II is given by:

$$\frac{K_{p,II}}{K_{p,I}} = \frac{\bar{D}_{2,I} (z_{1,I} - z_{2,I}) (z_{1,II} - z_{2,II}) \bar{D}_{2,II} / \bar{D}_{1,II}}{\bar{D}_{2,II} (z_{1,II} - z_{2,II}) (z_{1,I} - z_{2,I}) \bar{D}_{2,I} / \bar{D}_{1,I}} P_{s,II} / P_{s,I} \quad (27)$$

where $\bar{D}_i = K_{d,i} D_i$. As $K_{d,i}$ depends on r_p (Eq.(23) in Ref. [13]), also the $K_{p,i}$ ratio depends on r_p ; for example, $r_p = 0.5$ nm we get the following $K_{p,II}/K_{p,NaCl}$ ratios: $\text{NH}_4\text{NO}_3 - 5.8$, $\text{NH}_4\text{Cl} - 1.3$, $(\text{NH}_4)_2\text{SO}_4 - 0.38$, $\text{NaNO}_3 - 3.7$, and $\text{Na}_2\text{SO}_4 - 0.40$. In the limit $r_p \rightarrow \infty$ (no steric exclusion), these ratios change to 7.7, 1.8, 0.30, 3.7, and 0.28, respectively. According to the above approach, the difference in retention between NH_4NO_3 and NaCl (R_{obs} is smaller by about 0.1–0.15) is explained by at least sixfold higher sorption of NH_4NO_3 , whereas a higher retention of sulfates comparing with NaCl ($\Delta R_{\text{obs}} = 0.01-0.02$) is caused by ca. threefold smaller sorption of sulfates. Substituting K_p (Eq. (20) with steric, Φ_r and Born, $\Delta W_{B,r}$ terms only) into Eq. (27), for each electrolyte pair one gets a relation between r_p and ϵ_p depending on ϵ_p of one chosen electrolyte, for example, NaCl . The comparison of these relations for the studied electrolytes should inform about the reliability of the discussed model. According to them, it was found that the upper limit for $\epsilon_p(\text{NaCl})$ was 40; for higher values of $\epsilon_p(\text{NaCl})$, $\epsilon_p(\text{NH}_4\text{NO}_3)$ would exceed ϵ_b and $K_p(\text{NH}_4\text{NO}_3) > 1$. Lowering $\epsilon_p(\text{NaCl})$ to, for example, 20, ϵ_p for other electrolytes ranged from ca. 18 (NH_4Cl) to 27 (Na_2SO_4) (Fig. 6). Such high discrepancies in ϵ_p seems to be unrealistic for very dilute pore solutions. Unfortunately, it was not possible to reduce them by choosing another value of $\epsilon_p(\text{NaCl})$. To determine a probable r_p range, the effective thickness from Eq. (8a) and that from the pure water hydrodynamic permeability (Hagen-Poiseuille equation, $L_{p,w} \propto r_p^2/\delta$, Eq. (12) in Ref. [8]) were calculated. In Fig. 6, it is denoted as $\delta(\text{el.})$ and $\delta(\text{H}_2\text{O})$, respectively. It is seen that these quantities overlap in the range of r_p 0.4–0.7 μm , which corresponds to $\delta = 5-14$ nm. This range of δ includes the values obtained by Bowen et al. [8] for a NF membrane and chlorides (5.9–8.4 μm depending on the model assumptions).

4.1.1.2. The SPM-DE model

The consistency test of the SPM-DE model is based on the effective membrane thickness calculated from the electrolyte permeability (Eqs. (8a) and (19a)) using r_p and $\epsilon_p = f(r_p)$ shown in Fig. 5. It is seen (Fig. 7) that the discrepancy between electrolytes is significant – from $\delta = 5$ (NH_4NO_3) to 20 μm (NaCl). In the r_p range 0.6–0.8 nm, δ for NH_4NO_3 and NaNO_3 are practically the same (13.5 μm) and they cross $\delta(\text{H}_2\text{O})$ at $r_p = 0.7$ nm. Because of significant differences in δ , one may conclude that this approach still needs an improvement. Regarding the transport equation, one could take into account a coupling between cations and anions neglected in the extended Nernst-Planck equation (4) or apply the

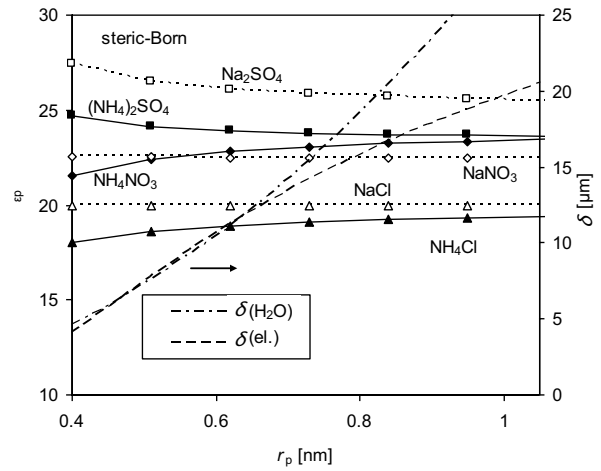


Fig. 6. The steric-Born exclusion: ϵ_p and δ versus r_p resulting from Eq. (26) for $\epsilon_{p,NaCl} = 20$, dashed line – δ from Eq. (8a), dash-dot line – δ from $L_{p,w}$.

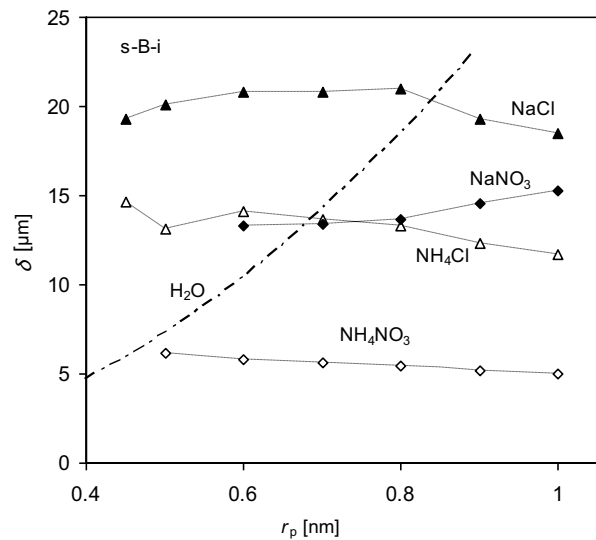


Fig. 7. The SPM-DE model – δ versus r_p ; ϵ_p is taken from Fig. 5; $\delta(\text{H}_2\text{O})$ is obtained from $L_{p,w}$.

Maxwell-Stefan equations which include such cross-effects. It is a question to what extent this coupling is important – for free solutions the cross coefficients become significant (>5%) for concentration higher than 0.03 M (NaCl , [57]), whereas the electrolyte concentration inside the membrane predicted by the dielectric exclusion is one order smaller. Another question is the applicability of the diffusive hindrance factor, derived from the basis of continuum hydrodynamics, to the estimation of ion diffusivities in the membrane nanopores.

4.1.1.3. The DPM model

Regarding the DPM model (only Donnan exclusion), using the values of $P_{s,u}$ in Table 3 and Eq. (8a) one got extremely large values of δ , which differed by an order of

magnitude – from 1,300 (NH₄NO₃) to above 13,000 μm (NaCl). It indicates that the incorporation of the dielectric and steric exclusions into that model is crucial for its proper functioning. It was checked that the DPM model with the included steric and Born exclusions yielded similar results as those shown in Fig. 6 for the SKK model.

5. Conclusions

The filtration models were tested using filtration data of ammonium and sodium salt solutions (nitrates, chlorides, and sulfates) through the commercial RO membrane (GE Water & Process Technologies). The data were characterized by the following series of electrolyte retentions: M₂SO₄ > MCl > MNO₃ (M = Na, NH₄) and NaA > NH₄A (A = Cl, NO₃).

As expected for the RO membrane, it was found that the convective part of the salt flux in all tested models was negligible. To obtain a satisfactory fit, a concentration dependence of electrolyte permeability was needed. The origin of this dependence did not play a role – dielectric exclusion caused by image forces, Donnan exclusion, or the assumed simple functions (Freundlich and Langmuir equations) yielded a similar goodness of the model fit.

In the model with dielectric (image force and Born effects) and steric exclusion, the partition coefficient is influenced by pore radius, r_p , and dielectric constant of pore solution, ϵ_p , in opposite directions. Thus, the same goodness of the model fit was obtained by many points (r_p, ϵ_p) forming a characteristic curve for each electrolyte. However, basing on these data, it was not possible to obtain a common value of effective membrane thickness for the electrolytes. Thus, this model needs a further improvement. It is suggested that two different values of ϵ_p should be used – one for the Born hydration energy estimation and the second one for the determination of the image force contribution. The additional information on ϵ_p can be obtained from the molecular dynamics simulations and from the EIS measurements. It is also pointed out that when expressing the ion flux in terms of internal quantities (concentration, electric potential), the image force component in the driving force should be taken into account.

Regarding the Donnan exclusion, its role in electrolyte exclusion was marginal, as indicated by enormously high values of the effective membrane thickness obtained for that type of exclusion.

Assuming that the electrolyte partition depends on the steric and Born exclusions only ($P_s = \text{constant}$), the effective membrane thickness obtained from the electrolyte permeabilities agreed with that from the water hydrodynamic permeability in the range 5–14 μm, which corresponded to pore radius, r_p , between 0.4 and 0.7 nm. However, the differences in the obtained values of ϵ_p for the studied electrolytes were much too high to be explained by those observed for free solutions of these electrolytes.

Symbols

A	–	Expression defined by Eq. (7)
c	–	Concentration of solute, mol/m ³
\bar{c}	–	Concentration of solute inside a membrane, mol/m ³

D_i	–	Diffusivity of species i in a solution, m ² /s
\bar{D}_i	–	Diffusivity of species i in a membrane, m ² /s
F	–	Faraday constant, 96,485 C/mol
J_v	–	Volume flux, m/s
$K_{c,i}$	–	Hindrance factor for convection of ion i
$K_{d,i}$	–	Hindrance factor for diffusion of ion i
K_p	–	Partition coefficient
k_c	–	Mass transfer coefficient, m/s
k_D	–	Ratio of diffusion coefficients, $k_D \equiv \bar{D}_i/\bar{D}_1$
L_p	–	Hydrodynamic permeability, m/s/Pa
l_p	–	Pore length, m
l_{pol}	–	Thickness of concentration polarization layer, m
n	–	Fitting parameter in Eq. (15)
P_s	–	Diffusional permeability of solute, m/s
\bar{P}_s	–	Diffusional permeability of solute inside a membrane, m/s
p	–	Pressure, Pa
R	–	Gas constant, 8.314 J/K/mol
R	–	Real retention coefficient
R_{obs}	–	Observed retention coefficient
r	–	Radius of stirrer, m
r_i	–	Radius of species i , m
$r_{\text{cav},i}$	–	Cavity radius of ion i , m
r_p	–	Pore radius, m
$r_{s,i}$	–	Stokes radius of ion i , m
S_v	–	Parameter defined as $S_v \equiv 1 - \sigma$
T	–	Absolute temperature, K
$\Delta W_{B,i}$	–	Dimensionless change in solvation energy resulting from the transfer of ion i from the external solution to the membrane pore solution, scaled with respect to RT
$W_{\text{im},i}$	–	Dimensionless image force contribution to the electrochemical potential of ion i , scaled with respect to RT
X_m	–	Concentration of fixed charges including their sign ($X_m \equiv z_m \bar{c}_m$), mol/m ³
X_p	–	Surface fraction of pores
x	–	Dimensionless coordinate, scaled with respect to l_p
z_i	–	Charge number of ion i
α_D	–	Temperature coefficient of D_i
α_p	–	Temperature coefficient of P_s
δ	–	$\delta \equiv l_p/X_p$ – effective membrane thickness, m
γ_{\pm}	–	Mean ionic activity coefficient on the molar scale
ϵ_b	–	Dielectric constant of bulk solution
ϵ_m	–	Dielectric constant of membrane pore walls
ϵ_p	–	Dielectric constant of pore solution
ν	–	Kinematic viscosity of solution, m ² /s
σ	–	Reflection coefficient
Φ_i	–	Steric exclusion term of ion i , $\Phi_i = (1 - r_{s,i}/r_p)^2$
φ	–	Electric potential in the membrane pore solution, V
$\Delta\varphi$	–	Potential difference between the pore and external solution, V
ω	–	Stirring speed, s ⁻¹

Subscripts

1 – cation, 2 – anion, f – feed, m – membrane or fixed charge, p – permeate or pore, s – solute, v – volume, w – water

References

- [1] A.B. Koltuniewicz, E. Drioli, *Membranes in Clean Technologies, Theory and Practice*, Wiley-VCH Verlag GmbH & Co. KGaA, Weinheim, 2008.
- [2] P. Schmidt, J. Micovic, P. Lutze, A. Górák, *Organic Solvent Nanofiltration – Challenges and Approaches of an Innovative Membrane Separation Process*, *Chem. Ing. Tech.*, 86 (2014) 602–610.
- [3] P. Marchetti, A.G. Livingston, Predictive membrane transport models for organic solvent nanofiltration: how complex do we need to be?, *J. Membr. Sci.*, 476 (2015) 530–553.
- [4] K.S. Spiegler, O. Kedem, Thermodynamics of hyperfiltration (reverse osmosis): criteria for efficient membranes, *Desalination*, 1 (1966) 311–326.
- [5] A.E. Yaroshchuk, Osmosis and reverse osmosis osmosis in fine-charged diaphragms and membranes, *Adv. Colloid Interface Sci.*, 60 (1995) 1–93.
- [6] E. Hoffer, O. Kedem, Hyperfiltration in charged membranes: the fixed charge model, *Desalination*, 2 (1967) 25–39.
- [7] T. Tsuru, S. Nakao, S. Kimura, Calculation of ion rejection by extended Nernst–Planck equation with charged reverse osmosis membranes for single and mixed electrolyte solutions, *J. Chem. Eng. Japan*, 24 (1991) 511–515.
- [8] W.R. Bowen, A.W. Mohammad, N. Hilal, Characterisation of nanofiltration membranes for predictive purposes – use of salts, uncharged solutes and atomic force microscopy, *J. Membr. Sci.*, 126 (1997) 91–105.
- [9] W.R. Bowen, J.S. Welfoot, Modelling the performance of membrane nanofiltration – critical assessment and model development, *Chem. Eng. Sci.*, 57 (2002) 1121–1137.
- [10] S. Lee, R.M. Lueptow, Membrane rejection of nitrogen compounds, *Environ. Sci. Technol.*, 35 (2001) 3008–3018.
- [11] K. Wesołowska, S. Koter, M. Bodzek, Modelling of nanofiltration in softening water, *Desalination*, 162 (2004) 137–151.
- [12] V. Hoshyargar, F. Fadaei, S.N. Ashrafizadeh, Mass transfer simulation of nanofiltration membranes for electrolyte solutions through generalized Maxwell–Stefan approach, *Korean J. Chem. Eng.*, 32 (2015) 1388–1404.
- [13] A. Szymczyk, P. Fievet, Investigating transport properties of nanofiltration membranes by means of a steric, electric and dielectric exclusion model, *J. Membr. Sci.*, 252 (2005) 77–88.
- [14] Y. Lanteri, P. Fievet, A. Szymczyk, Evaluation of the steric, electric, and dielectric exclusion model on the basis of salt rejection rate and membrane potential measurements, *J. Colloid Interface Sci.*, 331 (2009) 148–155.
- [15] A.E. Yaroshchuk, Dielectric exclusion of ions from membranes, *Adv. Colloid Interface Sci.*, 85 (2000) 193–230.
- [16] S. Bandini, D. Vezzani, Nanofiltration modeling: the role of dielectric exclusion in membrane characterization, *Chem. Eng. Sci.*, 58 (2003) 3303–3326.
- [17] S. Bouranene, P. Fievet, A. Szymczyk, Investigating nanofiltration of multi-ionic solutions using the steric, electric and dielectric exclusion model, *Chem. Eng. Sci.*, 64 (2009) 3789–3798.
- [18] W.R. Bowen, H. Mukhtar, Characterization and prediction of separation performance of nanofiltration membranes, *J. Membr. Sci.*, 112 (1996) 263–274.
- [19] D. Vezzani, S. Bandini, Donnan equilibrium and dielectric exclusion for characterization of nanofiltration membranes, *Desalination*, 149 (2002) 477–483.
- [20] G. Hagemeyer, R. Gimbel, Modelling the salt rejection of nanofiltration membranes for ternary mixtures and for single salts at different pH values, *Desalination*, 117 (1998) 247–256.
- [21] A. Santafé-Moros, J.M. Gozálvarez-Zafrilla, J. Lora-García, Nitrate removal from ternary ionic solutions by a tight nanofiltration membrane, *Desalination*, 204 (2007) 63–71.
- [22] A. Escoda, S. Déon, P. Fievet, Assessment of dielectric contribution in the modeling of multi-ionic transport through nanofiltration membranes, *J. Membr. Sci.*, 378 (2011) 214–223.
- [23] D.L. Oatley, L. Llenas, R. Pérez, P.M. Williams, X. Martínez-Lladó, M. Rovira, Review of the dielectric properties of nanofiltration membranes and verification of the single oriented layer approximation, *Adv. Colloid Interface Sci.*, 173 (2012) 1–11.
- [24] D.L. Oatley, L. Llenas, N.H.M. Aljohani, P.M. Williams, X. Martínez-Lladó, M. Rovira, J. de Pablo, Investigation of the dielectric properties of nanofiltration membranes, *Desalination*, 315 (2013) 100–106.
- [25] D.L. Oatley-Radcliffe, S.R. Williams, M.S. Barrow, P.M. Williams, Critical appraisal of current nanofiltration modelling strategies for seawater desalination and further insights on dielectric exclusion, *Desalination*, 343 (2014) 154–161.
- [26] A. Yaroshchuk, Non-steric mechanisms of nanofiltration: superposition of Donnan and dielectric exclusion, *Sep. Purif. Technol.*, 22–23 (2001) 143–158.
- [27] I. Koyuncu, Effect of operating conditions on the separation of ammonium and nitrate ions with nanofiltration and reverse osmosis membranes, *J. Environ. Sci. Health, Part A*, 37 (2002) 1347–1359.
- [28] F. Garcia, D. Ciceron, A. Saboni, S. Alexandrova, Nitrate ions elimination from drinking water by nanofiltration: membrane choice, *Sep. Purif. Technol.*, 52 (2006) 196–200.
- [29] A. Noworyta, T. Koziol, A. Trusek-Holownia, A system for cleaning condensates containing ammonium nitrate by the reverse osmosis method, *Desalination*, 156 (2003) 397–402.
- [30] G.M. Fu, T. Cai, Y. Li, Concentration of ammoniacal nitrogen in effluent from wet scrubbers using reverse osmosis membrane, *Biosyst. Eng.*, 109 (2011) 235–240.
- [31] D. Carter, L. Rose, T. Awobusuyi, M. Gauthier, F.H. Tezel, B. Kruczek, Characterization of commercial RO membranes for the concentration of ammonia converted to ammonium sulfate from anaerobic digesters, *Desalination*, 368 (2015) 127–134.
- [32] M.C. Wilbert, S. Delagah, J. Pellegrino, Variance of streaming potential measurements, *J. Membr. Sci.*, 161 (1999) 247–261.
- [33] P. Meares, Coupling of ion and water fluxes in synthetic membranes, *J. Membr. Sci.*, 8 (1981) 295.
- [34] P. Dechadilok, W.M. Deen, Hindrance factors for diffusion and convection in pores, *Ind. Eng. Chem. Res.*, 45 (2006) 6953–6959.
- [35] W.M. Deen, Hindered transport of large molecules in liquid-filled pores, *AIChE J.*, 33 (1987) 1409–1425.
- [36] A.L. Zydney, Stagnant film model for concentration polarization in membrane systems, *J. Membr. Sci.*, 130 (1997) 275–281.
- [37] A.E. Yaroshchuk, Rejection of single salts versus transmembrane volume flow in RO/NF: thermodynamic properties, model of constant coefficients, and its modification, *J. Membr. Sci.*, 198 (2002) 285–297.
- [38] S. Koter, Determination of the parameters of the Spiegler Kedem Katchalsky model for nanofiltration of single electrolyte solutions, *Desalination*, 198 (2006) 335–345.
- [39] K. Thibault, H.C. Zhu, A. Szymczyk, G.M. Li, The averaged potential gradient approach to model the rejection of electrolyte solutions using nanofiltration: model development and assessment for highly concentrated feed solutions, *Sep. Purif. Technol.*, 153 (2015) 126–137.
- [40] A.A. Rashin, B. Honig, Reevaluation of the Born model of ion hydration, *J. Phys. Chem.*, 89 (1985) 5588–5593.
- [41] C.S. Babu, C. Lim, A new interpretation of the effective Born radius from simulation and experiment, *Chem. Phys. Lett.*, 310 (1999) 225–228.
- [42] E.R. Nightingale Jr., Phenomenological theory of ion solvation. Effective radii of hydrated ions, *J. Phys. Chem.*, 63 (1959) 1381–1387.
- [43] Y. Miller, J.L. Thomas, D.D. Kemp, B.J. Finlayson-Pitts, M.S. Gordon, D.J. Tobias, R.B. Gerber, Structure of large nitrate-water clusters at ambient temperatures: simulations with effective fragment potentials and force fields with implications for atmospheric chemistry, *J. Phys. Chem. A*, 113 (2009) 12805–12814.
- [44] B. Ellis, R. Smith, Eds., *Polymers. A Property Database*, 2nd ed., CRC Press, Boca Raton, 2009.
- [45] X. Lefebvre, J. Palmeri, P. David, Nanofiltration theory: an analytic approach for single salts, *J. Phys. Chem. B*, 108 (2004) 16811–16824.
- [46] R.A. Robinson, R.H. Stokes, *Electrolyte Solutions*, Butterworths, London, 1959.

- [47] O. Kedem, A. Katchalsky, A physical interpretation of the phenomenological coefficients of membrane permeability, *J. Gen. Physiol.*, 45 (1961) 143–179.
- [48] P. Dydo, Transport model for boric acid, monoborate and borate complexes across thin-film composite reverse osmosis membrane, *Desalination*, 311 (2013) 69–79.
- [49] A. Escoda, Y. Lanteri, P. Fievet, S. Déon, A. Szymczyk, Determining the dielectric constant inside pores of nanofiltration membranes from membrane potential measurements, *Langmuir*, 26 (2010) 14628–14635.
- [50] J.O'M. Bockris, A.K.N. Reddy, *Modern Electrochemistry. An Introduction to an Interdisciplinary Area*, vol. 2, Plenum Press, New York, 1970.
- [51] H. Itoh, H. Sakuma, Dielectric constant of water as a function of separation in a slab geometry: a molecular dynamics study, *J. Chem. Phys.*, 142 (2015) 184703.
- [52] S. Deon, A. Escoda, P. Fievet, A transport model considering charge adsorption inside pores to describe salts rejection by nanofiltration membranes, *Chem. Eng. Sci.*, 66 (2011) 2823–2832.
- [53] P. Wang, A. Anderko, Computation of dielectric constants of solvent mixtures and electrolyte solutions, *Fluid Phase Equilib.*, 186 (2001) 103–122.
- [54] A. Efligenir, P. Fievet, S. Deon, R. Salut, Characterization of the isolated active layer of a NF membrane by electrochemical impedance spectroscopy, *J. Membr. Sci.*, 477 (2015) 172–182.
- [55] M. Montalvillo, V. Silva, L. Palacio, A. Hernández, P. Prádanos, Dielectric properties of electrolyte solutions in polymeric nanofiltration membranes, *Desal. Wat. Treat.*, 27 (2011) 25–30.
- [56] A.A. Hussain, S.K. Nataraj, M.E.E. Abashar, I.S. Al-Mutaz, T.M. Aminabhavi, Prediction of physical properties of nanofiltration membranes using experiment and theoretical models, *J. Membr. Sci.*, 310 (2008) 321.
- [57] D.G. Miller, Application of irreversible thermodynamics to electrolyte solutions. I. Determination of ionic transport coefficients l_{ij} for isothermal vector transport processes in binary electrolyte systems, *J. Phys. Chem.*, 70 (1966) 2639–2659.

Supplementary information:

S1. Thickness of concentration polarization layer, l_{pol}

The l_{pol} values calculated in various ways are listed in Table 4. The values obtained from the correlation equation (S1) (taken from Appendix A in Ref. [8]):

$$\frac{D_s}{l_{pol}} = k_c = 0.23 \left(\frac{\omega r^2}{\nu} \right)^{0.567} \left(\frac{\nu}{D_s} \right)^{0.33} \frac{D_s}{r} \quad (S1)$$

where r is radius of stirrer, ω – stirring speed, and ν – kinematic viscosity of solution are given for $\pm 10\%$ deviation of the set

value of stirring speed, ω (unfortunately, the stirrer was not equipped with a tachometer).

Only for NaCl the agreement between Eq. (S1) and the model fitting was observed. For other electrolytes, except for sulfates, Eq. (S1) predicted higher values of l_{pol} . l_{pol} could also be determined directly from Eqs. (26) and (12), if L_p and σ were known. Because of high retention, the contribution of solute to L_p should have been negligible and L_p should have been close to the water hydrodynamic permeability, $L_{p,w}$. Regarding σ , it was always higher than the real rejection coefficient, R (Fig. 4), thus for sulfates one could assume $\sigma = 1$, for chlorides it should have been not less than 0.99, only for ammonium nitrate σ could be > 0.93 . However, from the model fitting, it resulted that even for nitrates S_v ($S_v \equiv 1 - \sigma$) was less than 0.003, thus σ should have been higher than 0.997; a lower value of σ , for example, $\sigma = 0.93$, significantly decreased the goodness of fit. σ influences the calculated l_{pol} insignificantly – it was found that in the case of NH_4NO_3 the values of l_{pol} for $\sigma = 0.93$ and one differed by less than $20 \mu\text{m}$. In Table S1, mean values of l_{pol} for the sets of runs are given, calculated by minimizing the sum of squared errors:

$$SSE = \sum_k \left(\sum_i \left(\frac{J_{v,i}}{L_{p,w}} - (\Delta p - \sigma \Delta \pi_i) \right)^2 \right) \quad (S2)$$

where k numbers the runs, i – points of a given run; $\Delta \pi$ was calculated using the osmotic coefficients from Ref. [46]. l_{pol} obtained in this way is lower than that from Eq. (31) and from the model fits, except NH_4NO_3 .

S2. S_v and l_{pol} fitting

In the model fitting, in order to avoid meaningless values of S_v and l_{pol} , these quantities were substituted by a sigmoidal function Y ($Y = S_v, l_{pol}$):

$$Y = Y_{\min} + 0.5 \left(1 + \frac{y - 20}{\left(5 + (y - 20)^2 \right)^{1/2}} \right) (Y_{\max} - Y_{\min}) \quad (S3)$$

with y as a fitting parameter (for $y \rightarrow -\infty$ $Y \rightarrow Y_{\min}$, for $y \rightarrow \infty$ $Y \rightarrow Y_{\max}$). The following values of Y_{\min} and Y_{\max} were chosen: $S_{v,\min} = 0$, $S_{v,\max} = 1$, $l_{pol,\min} = 10$, and $l_{pol,\max} = 500 \mu\text{m}$.

Table S1

l_{pol} calculated for the sets of runs from: Eq. (S1) (for $\pm 10\%$ deviation of ω), Eq. (12) combined with (26), and the model fits. “x” denotes that the model fit is not significantly better than the SKK fit, “y” – no model solution is found for $r_p < 1.5 \text{ nm}$

Electrolyte	$D_{s,25}$ ($10^{-9} \text{ m}^2/\text{s}$) [46]	l_{pol} (μm)					
		Eq. (S1)	Eqs. (12) and (26)	SKK	cSKK	SPM-DE	DPM
NH_4NO_3	1.929	136–153	83 ± 4	84 ± 14	66 ± 6	58 ± 5	54 ± 5
NH_4Cl	1.994	138–154	75 ± 4	119 ± 11	111 ± 6	108 ± 7	109 ± 8
$(\text{NH}_4)_2\text{SO}_4$	1.530	126–141	82 ± 5	235 ± 4	x	y	x
NaNO_3	1.568	127–143	92 ± 3	83 ± 7	102 ± 3	111 ± 3	103 ± 3
NaCl	1.610	128–144	92 ± 3	123 ± 7	139 ± 5	139 ± 6	138 ± 5
Na_2SO_4	1.230	117–132	110 ± 4	150 ± 4	x	y	x